The Meteoritical Society

Meteoritics & Planetary Science 1–16 (2025)
doi: 10.1111/maps.70049

Löpönvaara: A new phosphorus-rich iron meteorite from Finland

Laura KOTOMAA[1]*, Markku VÄISÄNEN[2], Jussi S. HEINONEN[1,3], Ermei MÄKILÄ[4], Hugh O'BRIEN[5], and Arto PELTOLA[2]

[1]Geology and Mineralogy, Åbo Akademi University, Turku, Finland
[2]Department of Geography and Geology, University of Turku, Turku, Finland
[3]Department of Geosciences and Geography, University of Helsinki, Helsinki, Finland
[4]Department of Physics and Astronomy, University of Turku, Turku, Finland
[5]Geological Survey, of Finland, Espoo, Finland

***Correspondence**
Laura Kotomaa, Geology and Mineralogy, Åbo Akademi University, 20500 Turku, Finland.
Email: laura.kotomaa@abo.fi

(Received 26 August 2024; revision accepted 02 September 2025)

Abstract–Löpönvaara is a rare new phosphorus-rich iron meteorite find from Löpönvaara, Finland. The ~164 g meteorite was discovered in 2017 from the same area as the ungrouped Lieksa pallasite. Löpönvaara was classified as an ungrouped iron meteorite due to its unusually high concentration of P (>4 wt%), coupled with a moderate concentration of Ni (~11 wt%), and Ga–Ge abundances in the "III" range. The meteorite consists of ~75 vol% kamacite and ~22 vol% schreibersite, with accessory troilite (<0.1 vol%), and minor terrestrial weathering products. The kamacite in Löpönvaara occurs as three different types: (1) rare, large 2–5 mm partially resorbed clasts; (2) round, ≤0.5 mm partially resorbed clasts; and (3) small, several tens of μm to sub-μm exsolution blebs and globules in the matrix. Schreibersite occurs solely as microscopic matrix material in between the type (1) and (2) kamacite clasts. The lack of taenite and the overall compositional and textural features of Löpönvaara suggest that it retained its composition possibly from a P-rich portion of immiscible melt at late stages of fractional crystallization, but its textural features suggest that the meteorite suffered impact-related metamorphism. The meteorite has no close textural or compositional affinities, which makes it unique and an important target for future studies.

INTRODUCTION

Phosphorus is a common element in iron meteorites, typically occurring in phosphides that can range from μm-sized "rhabdites" to cm-sized masses. Phosphides commonly form a minor phase in iron meteorites, and the crystallization of vast amounts of schreibersite requires the melt to be considerably enriched in P. One way to enrich a Fe-Ni melt in P is through liquid immiscibility, and this process has been suggested to have played a key role in the formation of IIG irons, the most P-rich iron meteorites with bulk P contents ranging from 1.7 to 2.1 wt% (Wasson & Choe, 2009). Currently, only one iron meteorite has been reported to have a higher concentration of P than those of the IIG irons: the ungrouped Löpönvaara iron meteorite (Gattacceca et al., 2025, Kotomaa et al., 2023), which is the focus of this study. The only other ungrouped P-rich iron reported so far is the Soper iron, which contains 2.1 wt% P (Henderson & Perry, 1948), with its texture suggesting a possible impact-related origin (Buchwald, 1975).

The Löpönvaara meteorite was discovered on July 10, 2017, in Löpönvaara, ~10 km NE from the town of Lieksa, eastern Finland. The exact find location is at 63°24.221′N, 30°04.353′E (WGS84). The meteorite was found ~350 m from where the Lieksa pallasite was

discovered 6 weeks earlier (Chiappe, Ash, Luttinen, et al., 2023). After its discovery, the suspected Löpönvaara meteorite was sent to the Geological Survey of Finland (GTK), where it was briefly studied. The preliminary analysis indicated that the sample contained unusually high amounts of P compared to Fe for a meteorite, and it was suggested to be a "meteor-wrong." The sample was then further analyzed in the Department of Geography and Geology in the University of Turku (UTU). The presence of the meteoritic minerals kamacite and schreibersite strongly indicated that Löpönvaara is a P-rich iron meteorite (Kotomaa, 2022), and the sample was donated to the national meteorite collection of the Finnish Museum of Natural History (LUOMUS) on January 25, 2024. The meteorite was classified as an ungrouped iron due to its unique composition.

Prior to the official naming, the Löpönvaara meteorite had a field name "Lieksa 4," as it was the fourth suspected meteorite found near Lieksa in 2017. Since then, tens of small, metal-rich suspected meteorites have been recovered from the area, but only one of these has been chemically characterized: The first meteorite found from the area was named "Lieksa," and it was classified as an ungrouped pallasite based on metal and silicate abundances and chemistry (Gattacceca et al., 2024). This meteorite was reported to contain ~80% metal and ~20% silicate and oxide inclusions and was suspected to have originated from the non-carbonaceous domain of the solar nebula, and its isotopic fingerprint was found to be distinct from those of other pallasites and iron meteorites (Chiappe, Ash, Luttinen, et al., 2023). Löpönvaara's connection to Lieksa, or any other of these suspected meteorites, has yet to be studied and will be the topic of future research.

The main purpose of this study is to present and discuss results of the mineralogical and geochemical investigations of the ungrouped P-rich Löpönvaara iron meteorite. Phosphorus-rich iron meteorites are rare, and as of today, only eight P-rich iron meteorites have been identified, with most of them making up the low-Ni iron meteorite group IIG (Wasson & Choe, 2009). However, Löpönvaara differs drastically from those of the group IIG irons as well as from other iron meteorites both in composition and texture. Here, we report the chemical and textural characteristics of Löpönvaara and provide a discussion on the petrogenesis and classification of the meteorite based on a detailed characterization of its texture, mineralogy, and geochemistry.

ANALYTICAL METHODS

The 163.7 g meteorite was cut with a water-cooled diamond blade saw at GTK, and a 7.73 g piece was given to the finder of the meteorite. At UTU, the meteorite was cut first with a hand saw before it was identified as a meteorite, and later with a water-cooled cubic boron nitride blade. After cutting, the samples were cleaned and polished: a small 17 × 7.5 × 1 mm and ~15 g slice of the cut corner was mounted on an epoxy puck, while a larger 30 × 35 × 5 mm and 30.3 g slice was only polished but not mounted. In addition, a small ~10 g piece was ground to powder. During pulverization, the sample material was easily separated into two different fractions: round metallic granules (kamacite) and brittle, network-like matrix (schreibersite). The remaining 95.6 g main mass was donated to LUOMUS.

X-Ray Diffraction

Mineral identification was carried out using powder X-ray diffraction (XRD) at the Department of Physics and Astronomy, UTU. The XRD patterns were obtained using an Empyrean XRD diffractometer (Malvern Panalytical) in θ/θ configuration with a Bragg-Brentano^{HD} mirror and PIXcel^{3D} detector using Cu Kα radiation (λ = 1.54187 Å). The data were collected in the 2θ range of 20–100°, with a step size of 0.026° and a time of 300 s per step. The sample X-ray fluorescence was suppressed by energy filtering with the detector. The samples were set on a Si zero background plate, and the data was analyzed using the HighScore Plus v4.9 (Malvern Panalytical) and Match! (Crystal Impact) software.

Scanning Electron Microscopy

The bulk chemical composition and X-ray intensity maps of selected subareas were carried out using energy dispersive spectroscopy (EDS) analysis on the minerals, with backscattered electron (BSE) imaging using a field emission scanning electron microscope (FE-SEM) on the polished section and the meteorite slice. The SEM–EDS analyses were carried out using a Thermo Scientific Apreo S microscope equipped with an UltimMax 100 EDS detector (Oxford Instruments) at the Department of Physics and Astronomy, UTU. The polished section was coated with a ~10 nm thick layer of carbon prior to the analyses. Fe from EM-Tec RXS-36 M metals reference standard was used as an external standard for the analyses of the meteorite slice and the polished section. Three different mineral phases were identified using the phase analysis in Aztec 6.1 software (Oxford Instruments). The identified mineral phases were then analyzed from the polished section to obtain standardized phase compositions. Fe and Ni from EM-Tec RXS-36M metals reference standard, together with apatite and pyrite (for P and S abundances) from MAC Reference Standard 13205 were used to standardize these analyses. The standardization was done

TABLE 1. The average major and minor element compositions and standard of deviation of kamacite, schreibersite, and troilite in Löpönvaara.

Phase	Fe	Ni	P	S
Kamacite	86.0 ± 1.4	11.8 ± 1.2	1.1 ± 0.1	n.d.
Mid-sized clasts$_{n=21}$	86.6 ± 0.7	11.2 ± 0.6	1.1 ± 0.1	n.d.
Exsolved$_{n=7}$	84.0 ± 0.7	13.7 ± 0.7	0.9 ± 0.03	n.d.
Schreibersite$_{n=17}$	71.4 ± 1.1	12.3 ± 0.3	16.0 ± 0.1	0.2 ± 0.1
Troilite[a]$_{n=32}$	56.2 ± 4.2	n.r.	n.r.	30.3 ± 1.9
Bulk[b]	83.35	11.4	4.3	0.06

Note: All concentrations are in wt%. *n* is the number of analyses on different crystals (kamacite and troilite) or different spots in the matrix (schreibersite).

Abbreviations: n.d., not detected; n.r., not reported (due to known issue with inclusions distorting the results).

[a]The composition of troilite is calculated by deconvolving Ni and P from the results.

[b]Estimation of bulk composition calculated from modal abundances (vol%) of mid-sized kamacite, schreibersite, and troilite (with FeNi globules) determined by SE–-EDS phase analysis, and corrected to wt% according to their densities (kam = 7.9 g cm^{-3}; scb = 7.41 g cm^{-3}; tro = 4.60 g cm^{-3}).

with a beam current of 1.6 nA, and the instrument was operated at an accelerating voltage of 20 kV. The output count rates of all standardizations were ~95 kcps. We estimate the precision (coefficient of variation) of the method at or close to the coefficient of variation reported for the mid-sized kamacite clasts, which appear to be very homogeneous based on BSE imaging (Table 1).

For all the electron micrographs and elemental maps of the polished section and the meteorite slice, the instrument was operated at an accelerating voltage of 20 kV, apart from Figure 5 which was obtained with an accelerating voltage of 5 kV. A beam current of 1.2 nA was used for the meteorite slice, 2.0 nA for the elemental mapping and phase analysis of the polished section, and 1.6 nA for the detailed spectral analysis of the identified mineral phases of the polished section. The elemental maps of the polished section were obtained with an output count rate of ~170 kcps and >20 Mcts per frame, totaling to 396 frames. Similarly, the analysis of the meteorite slice consisted of 754 different frames, with an output count rate of ~180 kcps and >8 Mcts per frame. The phase analysis data used to determine phase abundances in the meteorite was obtained with an output count rate of ~120 kcps and >74 Mcts per spot. Compositional analysis of the mineral phases was obtained with an output count rate of ~95 kcps and >1.5 Mcts per spectrum area with a total of 72 spectrums from four different sites. The elemental compositions of the mineral phases were identified from four different sites in the polished section, and the phase compositions were calculated from a total of 61 spectral analyses (Tables S1–S4). All data were processed with the AZtec v6.1 software (Oxford Instruments).

Laser Ablation ICP-MS

The detailed trace element analysis from the main mineral phases was carried out with laser ablation single collector inductively coupled plasma mass spectrometry (LA-SC-ICPMS), using a Nu AttoM SC-ICPMS (Nu Instruments Ltd.) and an Analyte 193 ArF laser-ablation system (Photon Machines) at the Finnish Geosciences Research Laboratory (SGL) at the Geological Survey of Finland. The two fractions were analyzed separately due to their different compositions. For both the round granules and brittle network-like matrix, the laser was run at a pulse frequency of 10 Hz and a pulse energy of 5 mJ at 80% attenuation to produce an energy flux of 5.8 J cm^{-2} on the sample surface. The kamacite granules were analyzed with a 50 μm spot size, while a 35 mm spot size was used for the schreibersite. Each analysis was initiated with a 20-s baseline measurement followed by switching on the laser for 40 s for signal acquisition. Analyses were made using time-resolved analysis (TRA) with continuous acquisition of data for each set of points. GSE-1G glass was used as the primary external standard, with GSD-1G, BHVO-2G, and BCR-2G glasses as reference materials (Jochum et al., 2005) for quality control for both the kamacite and schreibersite analyses. GSD glass was used to obtain the standardized values for Ir, Pt, and Pd. In addition, known concentrations of reference materials (iron meteorites Elga, Sikhote Alin, Chinga, and Darinskoe) were used to process the data for the kamacite granules. No additional external reference materials were used for the analysis of the schreibersite phase. The one sigma error for the analyses uses $\sqrt{N}$ counting statistics on the signal and background counts, propagated through the equations. An assumed 1% relative uncertainty on the elemental concentrations of the reference material and a 3% relative uncertainty on the values of the internal standard (i.e., larger than coefficient of variation for the SEM–EDS analyses) is propagated throughout the calculations. These errors exceed the precision acquired by performing repeated

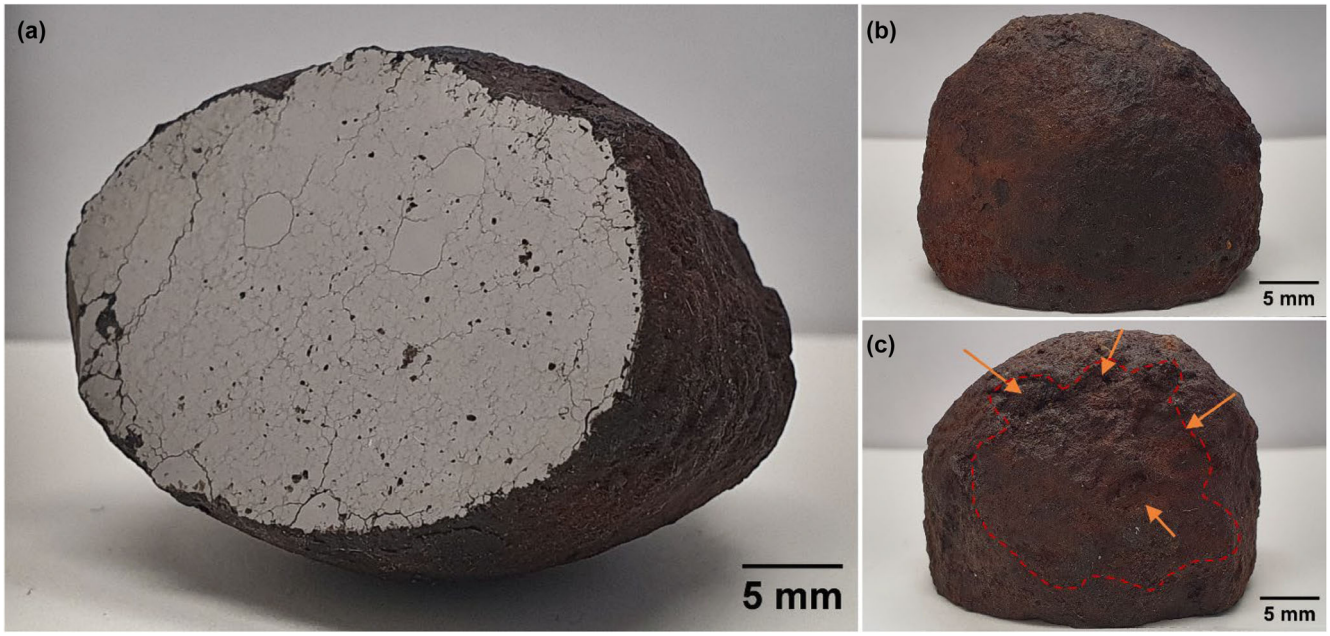

FIGURE 1. Löpönvaara polished end cut and weathered surface. (a) The weathered surface is covered in a ≤ 1 mm layer of rust, and the meteorite shows moderate rustiness along many fractures. (b) The smoother side of the weathered surface, vs (c) the opposite side that contains several pits (highlighted with orange arrows and red dashed line) that could be interpreted as strongly weathered remnant regmaglypts.

analyses on the above-mentioned standards in between sample analysis.

The isotope ^{57}Fe was selected as the internal standard using the average values for mid-sized kamacite and schreibersite obtained from the SEM–EDS analyses (uncertainty propagated as explained above). The measurements were performed on 39 isotopes covering 34 elements at low resolution ($\Delta M/M = 300$) using the fast-scanning mode. The data reduction was handled using the software GLITTER™ (Van Achterbergh et al., 2001), which allows baseline subtraction, integration of the signal over a selected time-resolved area, and data quantification using known concentrations of the external and internal standards. A total of 19 elements above detection limits were recorded from the kamacite phase (Table S5), and 15 from schreibersite (Table S6), with a 99% confidence.

RESULTS

External Morphology

The meteorite has a rounded shape, and the dimensions of the main mass (95.6 g) are approximately 3 × 3.5 × 2.5 cm (Figure 1). The weathered surface of the meteorite is covered by a thick (≤1 mm) crust of terrestrial oxides. Overall, the meteorite shows moderate rustiness, and rust can also be observed on the cut surface along fractures (Figure 1a). Furthermore, one side of the meteorite has a more irregular shape and contains rounded pits of approximately 2 mm in diameter (Figure 1c). At least some of the pits may represent remnant regmaglypts, but it is difficult to discern with certainty as weathering has strongly affected the surface features.

Primary Textures and Mineral Chemistry

The XRD analysis of the pulverized material identified the main mineral phases as kamacite (α-(Fe, Ni)) and schreibersite ((Fe,Ni)$_3$P; Figure S1), which make up roughly 96 vol% of the sample based on SEM–EDS analysis. The primary texture of the meteorite is dominated by round, small, metallic kamacite clasts set in a much more fine-grained and brittle schreibersite matrix (Figure 2), which also contains exsolved kamacite and minor Fe-sulphide (Figure 3). The great majority of the kamacite clasts have diameters ≤0.5 mm, although a few larger clasts can be seen on the polished end cut. The analytical data of the phases is compiled in Table 1. Full SEM–EDS analysis datasets of the three different mineral phases are provided in Tables S1–S4.

Kamacite

Kamacite is a major mineral phase in the meteorite, constituting ~75 vol% of the sample (Figure 2). It occurs as three different anhedral forms: (1) rare large, 2 to 5 mm partially resorbed clasts (Figure 4e–f); (2) round,

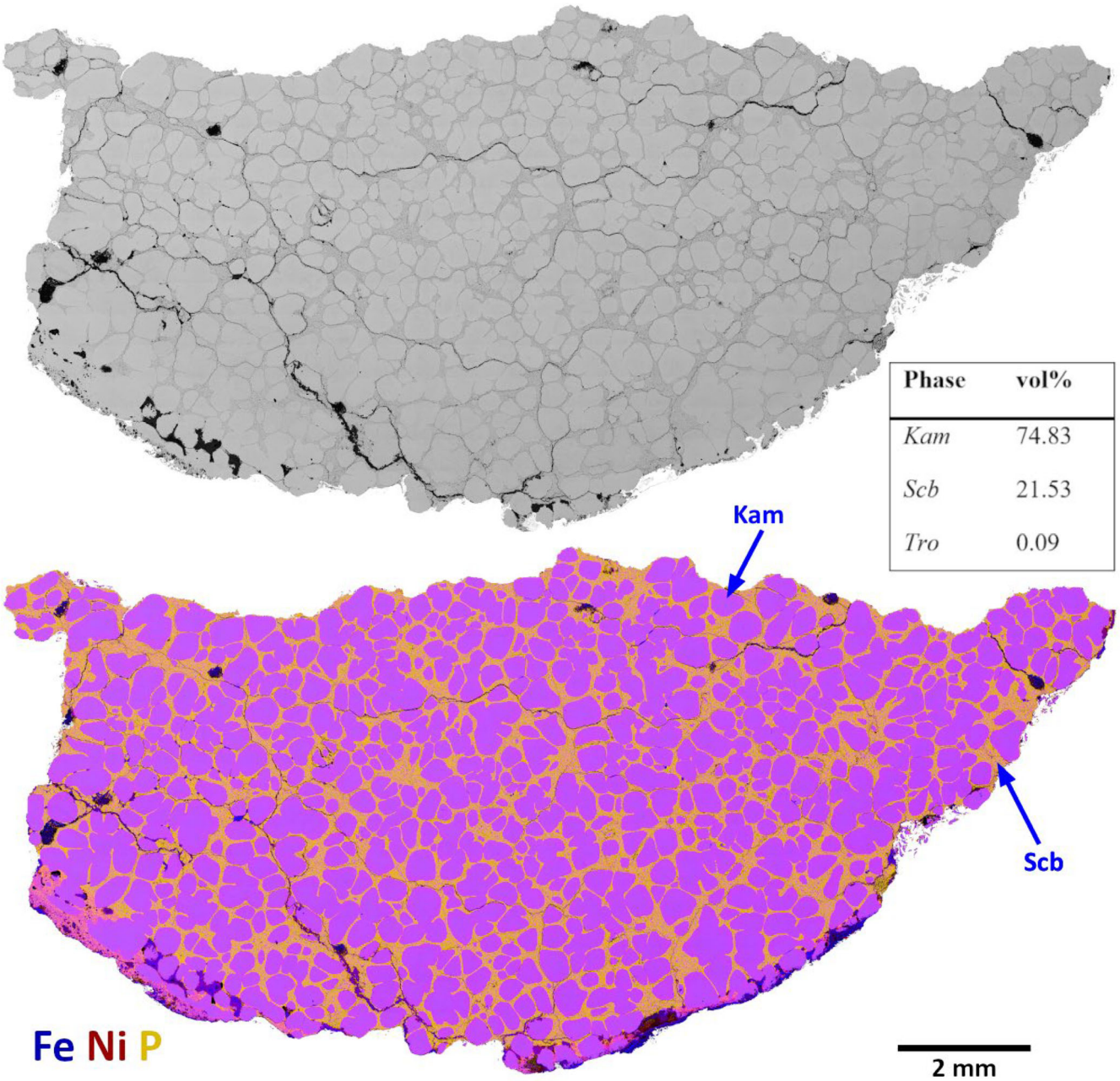

FIGURE 2. BSE micrograph (upper) and EDS elemental map (lower) of the polished section, showing the texture of the meteorite and the distribution of the main elements Fe, Ni, and P. Iron and Ni occur both in the round granules and within the matrix, while the great majority of P is in the web-like matrix. The round granules are kamacite (Kam), while the matrix consists largely of schreibersite (Scb). The micrograph is compiled of 396 individual frames.

≤ 0.5 mm partially resorbed clasts (referred to as "mid-sized kamacite" from here on); and (3) small, several tens of μm to sub-μm size exsolved blebs and globules in the matrix (Figures 3 and 4a–d).

Both the large and mid-sized kamacite clasts show rounded, often "scalloped" contacts with the matrix. The exsolved kamacites typically show parallel exsolution textures in different areas, although not always. This study reports standardized data only for the mid-sized and exsolved kamacite (Table 1). However, preliminary (non-standardized) data indicated that the composition of the large and mid-sized clasts differs slightly in terms of P (~40% lower in the large clasts) and that the Fe and Ni contents are within the standard deviation of the whole dataset. In general, kamacite is homogeneous in composition and contains ~1 wt% P (Table 1).This is higher

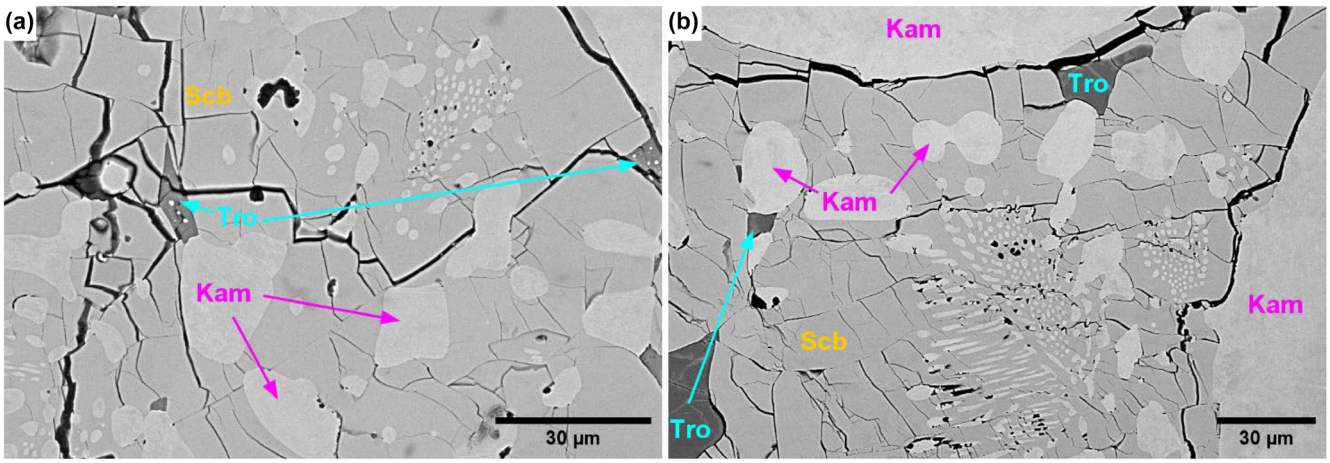

FIGURE 3. BSE images showing the details of the matrix texture in the meteorite. Schreibersite (Scb) shows brittle fracturing throughout the sample and makes up a web-like matrix between the mid-sized kamacite clasts (Kam). The matrix contains minor amounts of troilite (Tro) and large amounts of exsolved kamacite with different textures and a higher concentration of Ni compared to the mid-sized kamacite clasts. Most of the troilite in Löpönvaara contains sub-µm high-Ni FeNi globules (as in b), and globule-free troilite (as in a) is very rare in the sample.

than reported for the metal phase in other P-rich irons (~0.1–0.3 wt%; Hofmann et al., 2009, Groeneveld, 1959). A relatively higher P content in Löpönvaara kamacite is possible, but should be taken with caution since we did not have a proper standard to analyze phosphorus in metal, and the matter requires further research. The mid-sized kamacite clasts contain ~86 wt% Fe, 11 wt% Ni, and 1.1 wt% P on average, while the exsolved kamacite contains relatively more Ni (13.7 wt%) and less P (0.9 wt%).

Schreibersite

Schreibersite constitutes ~22 vol% of the meteorite (Figure 2). It occurs as a heavily fractured phase, filling the spaces between the large and mid-sized kamacite clasts (Figures 3 and 4a–d). The schreibersite grain boundaries are not clearly discernible, and it forms a network-like matrix that contains an abundance of exsolved kamacite. In addition, troilite occurs in small quantities at schreibersite-kamacite grain boundaries. Much like the kamacite, the schreibersite phase is also very homogeneous, and contains on average ~71 wt% Fe, 12 wt% Ni, and 16 wt% P (Table 1).

Troilite (with FeNi globules)

Troilite occurs in the Löpönvaara meteorite in very small quantities (<0.1 vol%), and it can be found in interstitial domains within the schreibersite-matrix. Most of the troilite has a grain size of ≤30 µm (Figure 3a), although several slightly larger (~30–60 µm) crystals can also be observed (Figures 3b and 4c,d). Almost all troilite in the meteorite is zoned and contains sub-µm globules of possibly exsolved high-Ni FeNi phase (Figure 5) that has a taenitic composition (~60 wt% Fe, and 35 wt% Ni based on SEM spectral analysis). These globules also contain P in similar abundances to the kamacite phase, and some S. Globule-free troilite (Figure 3b) is very difficult to find in the sample, and we were not able to analyze any of them during the spectral analysis session with SEM. The prevalent occurrence of the small globules in the analyzed troilite affects its composition to some degree. Deconvolving Ni and P from the analyzed troilites gives the troilite phase an average composition of 30 wt% S and 56 wt% Fe (Table 1), but these values should also be taken with caution. Furthermore, the troilite phase seems very heterogeneous in composition: The compositional variability of the analyses is outside the estimated precision for SEM–EDS and represents real sample heterogeneity, likely caused by the variable occurrence of the FeNi globules.

Terrestrial Weathering

Signs of terrestrial weathering are moderate in the interior of Löpönvaara but severe on the outer layer, which is completely covered in rust. Based on the phase analysis data, the different products of terrestrial weathering make up ~2 vol% of the inside of the meteorite. Because Löpönvaara is highly fractured, the oxidized FeNi and terrestrial oxidation phases occur commonly in the fractures. These veinlets are more abundant towards the external surface, but they fill the fractures in the inner parts of the meteorite as well.

Bulk Chemistry

The Löpönvaara meteorite is characterized by moderate Ni, high P, and low S abundances. Iron, P, and

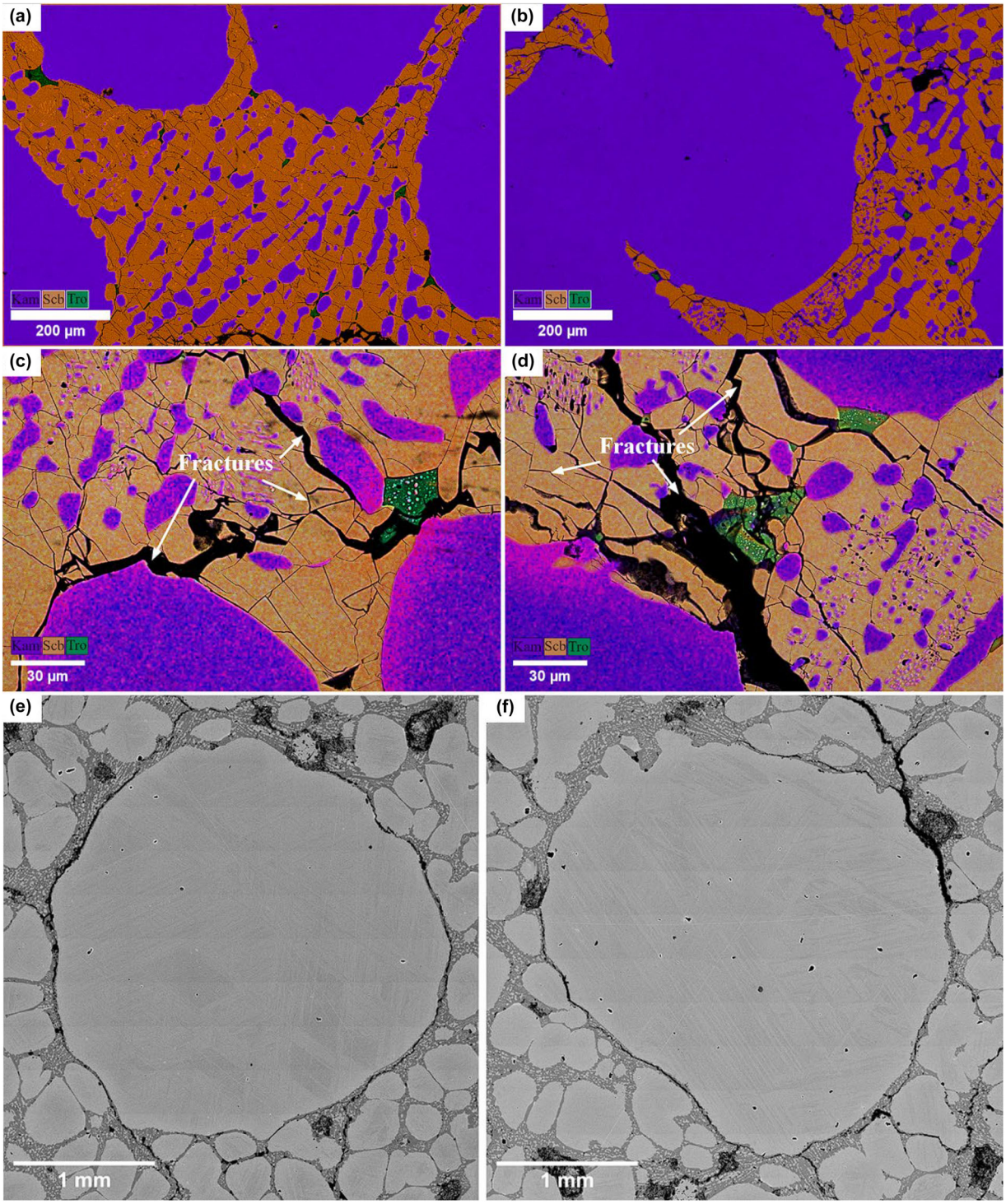

FIGURE 4. (a, b) EDS phase maps of the texture of Löpönvaara. Kamacite occurs as round, ≤500 µm clasts and exsolved globules of varying shapes and sizes in the matrix. The matrix consists mainly of highly fractured schreibersite with a network-like texture. (c, d) EDS layered elemental maps showing the details of the matrix texture. Troilite occurs in small amounts as ≤30 µm crystals and often contains sub-µm high-Ni FeNi globules. (e, f) BSE micrographs showing examples of large kamacite clasts in the meteorite. These clasts are much larger than the average kamacite clasts, and they have a similar, rounded texture with "scalloped" contacts with the matrix and mid-sized kamacite clasts. Micrographs compiled from 30 to 40 individual frames. Kam, kamacite; Scb, schreibersite; Tro, troilite.

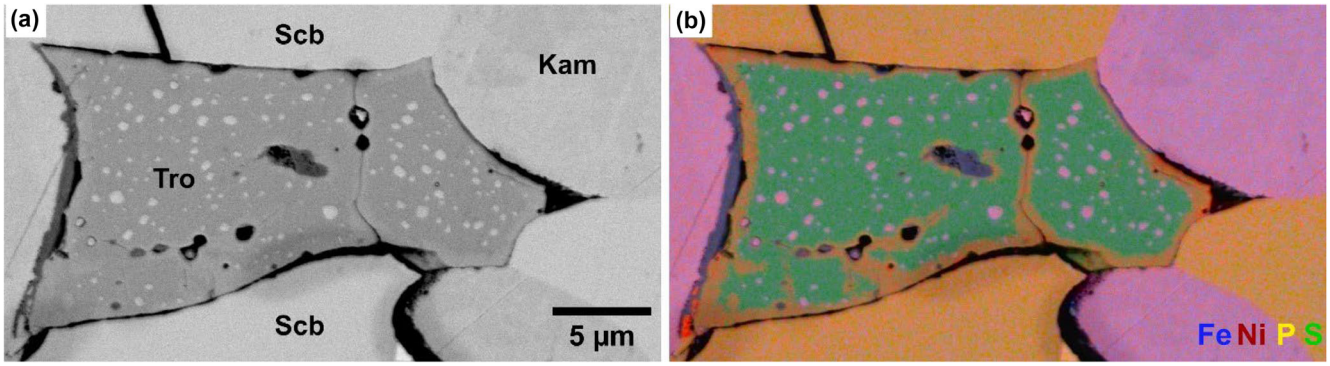

FIGURE 5. (a) BSE image and (b) EDS layered elemental map showing the texture of troilite in Löpönvaara. Most of the troilite contains sub-μm FeNi globules with taenitic composition. Note also the zoning texture in troilite; the troilite grain boundaries are enriched in Ni from the surrounding kamacite and schreibersite.

S abundances of the main mineral phases were determined by standardized SEM–EDS analyses. These results show that the meteorite is highly enriched in P and depleted in S, with the bulk P abundance of the meteorite totaling to ~4.3 wt%, while the bulk S abundance is 0.06 wt% (Table 1). The bulk main element abundances were calculated based on the standardized SEM–EDS main element abundances from the mid-sized kamacite phase (Table 1) together with the phase analysis results shown in Figure 2, which were corrected to wt% according to their specific densities (see details in Table 1 footnote). The terrestrial oxidation phases were left out of the calculation.

Trace Element Chemistry

The trace element abundances of kamacite and schreibersite were determined by LA-SC-ICPMS from 60 mid-sized kamacite clasts and 30 different spots in the schreibersite matrix. The main and trace element abundances in the meteorite's two major phases are reported in Table 2. Figure 6 shows selected trace element abundances in Löpönvaara's kamacite phase plotted against Ni with other iron meteorite groups in comparison. The LA-ICPMS data for individual analysis spots from the kamacite and schreibersite phases are given in Table S5 and S6. The siderophile trace element data from kamacite in Löpönvaara is normalized to CI chondrite abundances and compared with other iron groups in Figure 7.

TABLE 2. Combined elemental concentrations and their standard deviations in the mid-sized kamacite clasts and schreibersite matrix.

Element	Kamacite (mid-sized) (n = 60)	Schreibersite (n = 30)
Fe (wt%)	86.6 ± *0.7*	71.4 ± *1.1*
Ni (wt%)	11.2 ± *0.6*	12.3 ± *0.3*
P (wt%)	1.1 ± *0.1*	16.0 ± *0.1*
S (wt%)	n.d.	0.2 ± *0.1*
Co (wt%)	0.41 ± *0.01*	0.34 ± *0.02*
Cr	317 ± *10*	419 ± 180
Cu	62 ± *3*	57 ± 32
Ga	10.6 ± 0.6	3.4 ± 1.2
Ge	5 ± 1	1.1 ± 0.8
Mn	5.3 ± 0.9	4.9 ± 2.3[a]
Ir	5.6 ± *1.5*	<0.04[b]
Pt	4.5 ± *0.7*	<0.06[b]
As	4.4 ± 1.5	5.9 ± 3.4
Mo	2.6 ± 0.6	2.7 ± 1.7
Pd	1.5 ± *0.3*	2.3 ± 1.4
V	1.0 ± 0.2	1.6 ± 0.9
W (ppb)	289 ± 140	<42[b]
Re (ppb)	106 ± 54	<400[b]
Au (ppb)	142 ± 51	84 ± 72
Pb (ppb)	14 ± 13	150 ± 130[c]

Note: Results in ppm except where indicated. Results in wt% measured with SEM–EDS; results in ppm and ppb measured with LA-SC-ICPMS. ± Values in *italics* are within analytical precision.
Abbreviations: n.d., not detected; SEM-EDS, scanning electron microscope–energy dispersive spectroscopy.
[a]Excluding two outliers with >29 ppm.
[b]Values below detection limit.
[c]Excluding one outlier with >1440 ppb.

DISCUSSION

Comparison with Other Iron Meteorites

Löpönvaara is a unique discovery that currently has no direct textural or mineralogical analogues to other iron meteorites. It has the highest bulk P concentration ever reported for an iron meteorite, with the meteorite consisting of ~4.3 wt% P. Furthermore, Löpönvaara's trace element concentrations do not plot consistently with any other iron group, although based on Ga–Ge systematics, the meteorite plots within the "III" range.

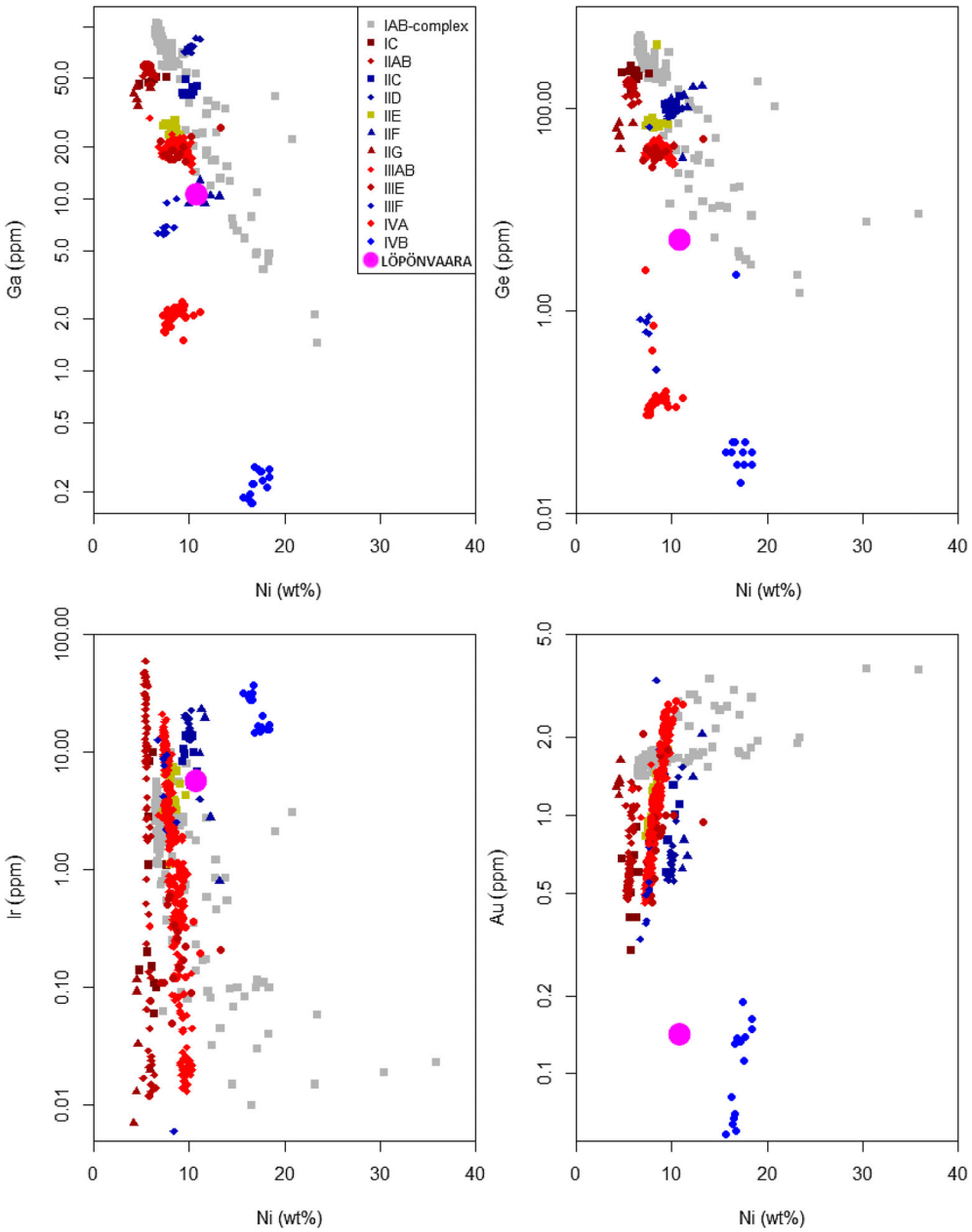

FIGURE 6. Compilation of data of (a) Ga (ppm) versus Ni (wt%), (b) Ge (ppm) versus Ni (wt%), (c) Ir (ppm) versus Ni (wt %), and (d) Au (ppm) versus Ni (wt%) for fractionally crystallized and silicate-rich irons, and the Löpönvaara iron meteorite determined from the mid-sized kamacite clasts. Löpönvaara is represented with a purple circle. Data combined from LA-SC-ICPMS and INAA analysis results of 651 irons reported in Scott et al. (1973); Scott and Wasson (1976); Buchwald (1975); Kracher et al. (1980); Esbensen et al. (1982); Malvin et al. (1984); Wasson et al. (1989, 1998); Wasson and De Bon (1998); Wasson (1990, 1999, 2011, 2016); Wasson and Richardson (2001); Wasson and Kallemeyn (2002); Wasson and Huber (2006); Wasson et al. (2007); Walker et al. (2008); Wasson and Choe (2009); Weisberg et al. (2009); Garvie (2012); Ruzicka et al. (2015); Wasson (2017); Gattacceca et al. (2019, 2020, 2024); Hilton et al. (2020); Moutinho et al. (2022); Tornabene et al. (2020, 2023); Chiappe et al. (2023); Zhang et al. (2022) and Table 2.

Only a handful of P-rich iron meteorites have been identified, namely the ungrouped Soper iron (Buchwald, 1975), and the IIG iron meteorite group that consists of only six members (Wasson & Choe, 2009). The Soper iron is currently the only other ungrouped P-rich iron in addition to Löpönvaara, with its bulk composition consisting of 2.08 wt% of P and 5.70 wt% Ni (Table 3; Henderson & Perry, 1948; Wasson & Schaudy, 1971). Both Soper and Löpönvaara are ataxites, with kamacite and schreibersite as their two main phases. Soper

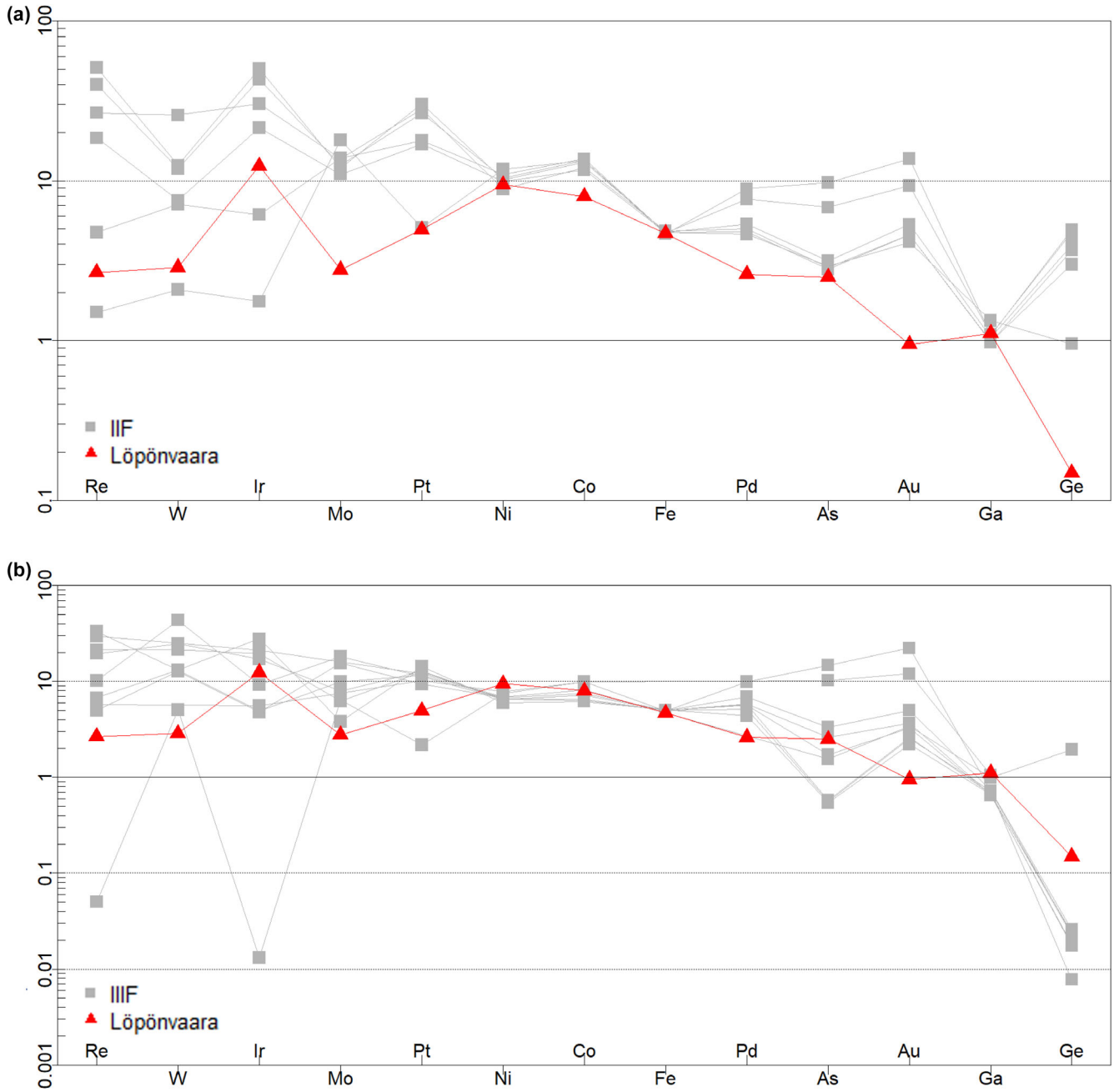

FIGURE 7. CI chondrite-normalized siderophile element abundances of Löpönvaara compared to groups (a) IIF and (b) IIIF. Data from Hilton et al. (2020) and Zhang et al. (2022). CI chondrite normalization data from Lodders et al. (2025).

contains no taenite, troilite, or other meteoritic minerals (Henderson & Perry, 1948). The texture of Soper consists of 10–100 μm mosaic equiaxial kamacite, with 10–100 μm irregular dendritic schreibersite surrounding the kamacite grain boundaries, and it was interpreted to have formed upon fast solidification possibly due to one or two reheating events (Buchwald, 1975). This hypothesis was supported by Soper's noble gas concentrations, which were shown to have substantial loss of tritium (Hintenberger et al., 1967), relative to those of unaltered irons.

The IIG irons are hexahedrites with much lower concentration of Ni (~4.2–5.7 wt%; Table 3) compared to Löpönvaara, although they consist of the same main mineral phases. The IIG irons, which are considered the most P-rich iron group with 1.7–2.1wt% bulk P, are believed to be the end product of very slow cooling in a planetesimal core (Wasson & Choe, 2009). They consist

TABLE 3. Compositional data of Löpönvaara compared to the Soper iron and group IIG irons.

Meteorite	Ni (wt%)	Co (wt%)	P^{bulk} (wt%)	S^{bulk} (wt%)	Ir	Ga	Ge	Au	As	Cu	Cr	References
Löpönvaara	11.2	0.41	4.3	0.06	5.6	10.6	5.0	0.142	4.4	62	317	This paper
Soper	5.66	0.54	2.1		0.011	9.7	10.8					Henderson and Perry (1948); Wasson and Schaudy (1971)
Group IIG												
Tombigbee R.	4.18	0.53	1.8	<0.1	0.007	40.6	62.5	1.281	16.8	86	10	Wasson and Choe (2009)
Guanaco	4.43	0.51			0.013	44.7	71	1.194	14.6	93	14	
Twannberg	4.46	0.52	2.0	0.01	0.092	37.6	51.4	1.364	17.8	86	16	
Bellsbank	4.50	0.53	2.1	~0.1	0.120	37.6	53.9	1.328	17.4	87	12	
La Primitiva	4.64	0.54	1.7	0.2	0.033	34.5	38.6	1.633	19.9	97	13	

Note: Results in ppm except where indicated. Both Soper and IIG data obtained with INAA, except for P and S concentrations in IIG irons, which were calculated via modal concentrations (Wasson & Choe, 2009). Löpönvaara main element data (except Co) was collected by scanning electron microscope–energy dispersive spectroscopy (SEM–EDS), and trace element data (+ Co) by LA-ICPMS.

of very large kamacite with hieroglyphic schreibersite inclusions, the latter accounting for 11–14 vol% of the IIG irons (Wasson & Choe, 2009). In Löpönvaara, the abundance of schreibersite is even greater than this, totaling up to ~22 vol%. Both Löpönvaara and IIG irons appear to be similarly depleted in S. The low S concentration of the IIG group has been suggested to be the result of liquid immiscibility occurring in the IIAB–IIG parent body: The IIG irons likely crystallized from the P-rich portion of the magma, while the IIAB irons crystallized from the S-rich portion (Wasson & Choe, 2009). The sparse textural and compositional (Table 3) similarities between Löpönvaara, the Soper iron, and the IIG irons suggest that a genetic relationship between these meteorites is not likely.

Although Löpönvaara has no direct compositional or textural analogues, it exhibits similarities in the chemical composition of certain elements to other iron groups. The iron meteorite groups with overall similar highly siderophile element (HSE) abundances (except for Os, Rh, and Ru that were not detected) compared to Löpönvaara are the groups IIF and IIIF (Figure 7), which can be used to give insights about the formation and evolution of the Löpönvaara parent body. Both groups share similarities with the overall HSE pattern with Löpönvaara, specifically in the Ir and Ga concentrations. In addition, both IIF and IIIF groups exhibit similar moderately to highly refractory siderophile element abundances (especially in terms of Ni, Co, W, and Pd) which suggests that their parent bodies accreted from similar precursor material. Both IIF and IIIF groups are considered to be fractionally crystallized irons, but the IIIF parent body likely experienced a complex parent body evolution after fractional crystallization (e.g., Zhang et al., 2022), which also seems likely in the case of Löpönvaara.

While Löpönvaara shares some compositional similarities with other iron groups, its overall siderophile element pattern is unique. Another unusual meteorite that exhibits an unique siderophile element pattern is the ungrouped Lieksa pallasite, which was discovered just ~200 m from where Löpönvaara was found (Chiappe, Ash, Luttinen, et al., 2023; Gattacceca et al., 2024, 2025). The Lieksa meteorite was reported to host compositional similarities with the IIC and IIF irons, but also with the IID irons (Chiappe, Ash, Luttinen, et al., 2023). When comparing the compositional data of these two unique meteorites (Figure 8), Löpönvaara shows similar compositions with Lieksa namely in Fe, Ni, Ir, Co, Pd, and As concentrations, but its Au, Ga, and Ge concentrations differ from those of Löpönvaara. In addition, Lieksa's metal phase consists of the intergrowth of kamacite and taenite, and the meteorite lacks phosphides. Instead, Lieksa contains olivine and spinel inclusions, and accessory amounts of troilite. Naturally, these compositional similarities are not enough to genetically link these two unusual meteorites without further studies.

Crystallization History

Löpönvaara is unusual in that schreibersite is one of its two major mineral phases, making up approximately 22 vol% of the meteorite, which is far more than in any other P-rich iron. Schreibersite occurs commonly in iron meteorites either as large, hieroglyphic inclusions or small, microscopic crystals, or rod-like crystals also known as "rhabdites." In Löpönvaara, schreibersite occurs as a highly fractured and brittle, uniform phase, located in between the mid-sized and large kamacite clasts. The large and mid-sized kamacite clasts likely represent entrained, partially resorbed clasts as they

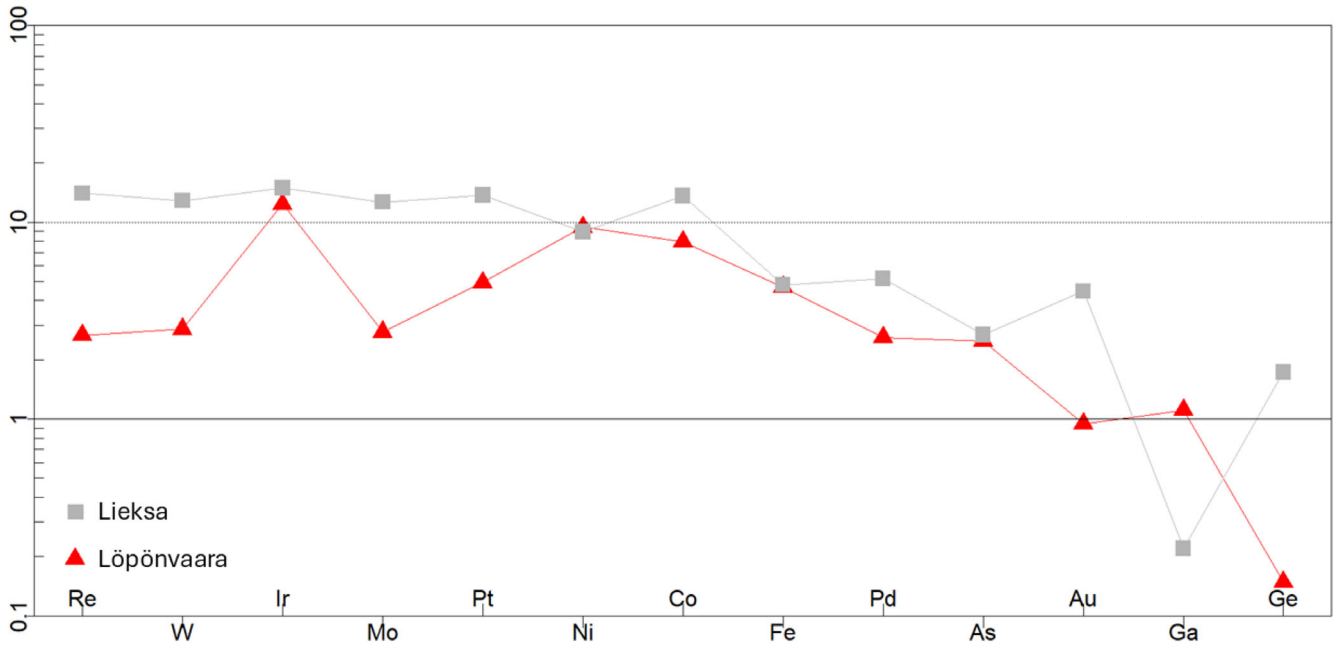

FIGURE 8. CI-chondrite normalized siderophile element abundances of Löpönvaara compared to the ungrouped Lieksa pallasite. Lieksa data from Chiappe, Ash, Luttinen, et al. (2023).

exhibit a rounded shape, and they show a scalloped-like contact with the schreibersite-matrix. Furthermore, the meteorite contains small amounts of zoned troilite which has a very heterogeneous composition, as it often contains sub-μm FeNi droplets with a taenitic composition based on its high Ni concentration. Overall, these globules and zoning in troilite together with the brittle deformation in schreibersite suggest that the meteorite experienced large-scale deformation, possibly due to a shock event on its parent body. Any other shock features, such as Neumann deformation lines, were not found from the meteorite although they were previously reported (Kotomaa et al., 2023).

Like Soper, Löpönvaara is a highly unequilibrated iron meteorite. Its cooling rate must have been rapid so that no homogenization could take place. This also allowed the meteorite to retain its texture with a very small grain size. Meanwhile, the major element abundances of Löpönvaara suggest that the meteorite likely obtained its original composition from a magma that was highly enriched in P and depleted in S, raising the question of whether liquid immiscibility could have played a role in Löpönvaara's parent body and explain the very high concentration of P in this meteorite. It is possible that Löpönvaara retained its composition from a magma that went through immiscibility, as the enrichment of P is similarly high to IIG irons. We emphasize, however, that Löpönvaara's texture most likely originates from a later reheating event that altered the meteorite drastically.

The growth and textures of phosphides in different types of iron meteorites have been studied in detail (Doan & Goldstein, 1969, 1970; Goldstein & Doan Jr, 1972; Romig & Goldstein, 1980, 1981) to understand the effect of P on the formation of different textures in iron meteorites. Overall, it has been suggested that in irons with >6.5 wt% Ni and a high concentration of P, kamacite forms by the reaction path γ-(Fe,Ni) (taenite) + Ph (phosphide; schreibersite) → α-(Fe,Ni) (kamacite) + γ(Fe, Ni) + Ph (Doan & Goldstein, 1969). Kamacite nucleates initially on taenite grain boundaries with little or no undercooling, and the addition of >0.1 wt% P promotes the rapid nucleation of kamacite at higher temperatures and lowers the amount of undercooling needed to nucleate kamacite homogeneously (Goldstein & Doan, 1972). Microscopic schreibersite such as the one in Löpönvaara nucleates primarily on the kamacite/taenite interfaces as the meteorite enters the $\alpha + \gamma$ + Ph phase field at low temperatures (Figure 9). When the temperature drops from 650 to 400°C, both kamacite and schreibersite grow at the expense of taenite, which can result in the complete absorption of taenite (Doan and Goldstein, 1969; Goldstein and Doan Jr, 1972). The kamacite/taenite interfaces provide a supply of both Ni from taenite and P from kamacite and are thus an ideal nucleation site for schreibersite (Reed, 1965). The amount of schreibersite produced this way can be extensive (Doan & Goldstein, 1969). Thus, it is possible that the very high amount of schreibersite in Löpönvaara formed at the expense of the complete absorption of taenite from

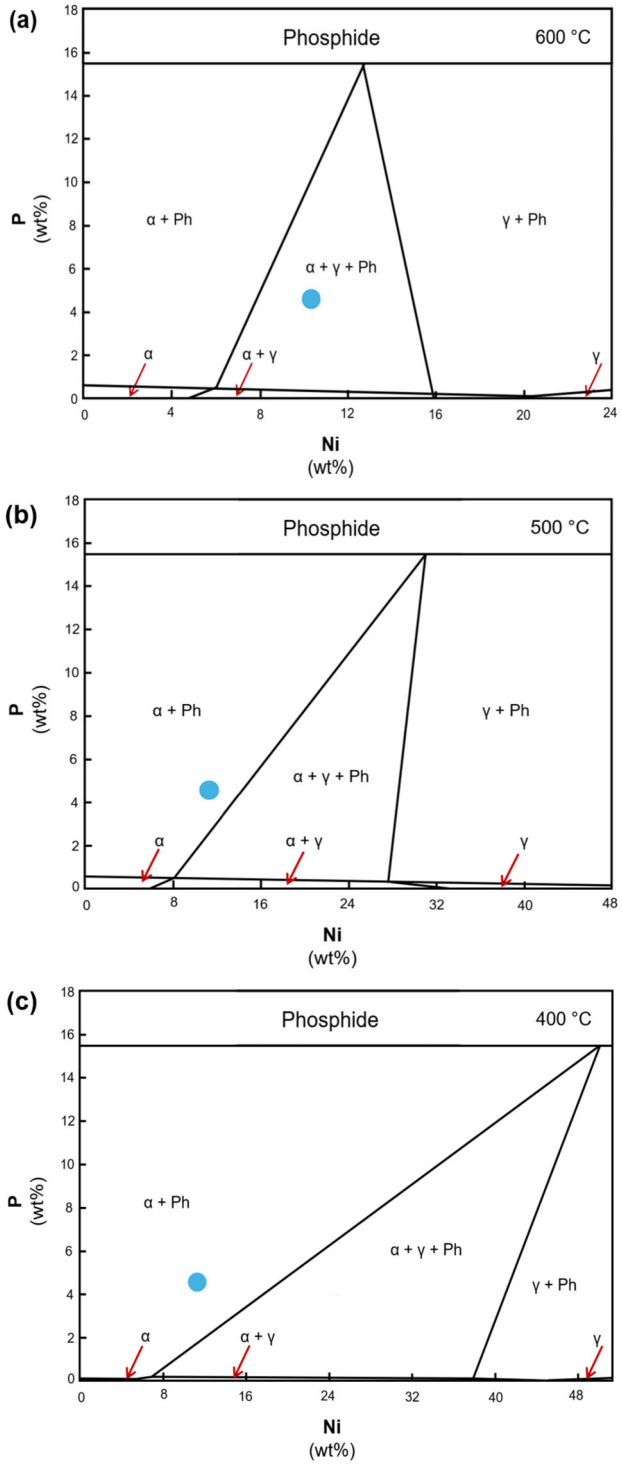

FIGURE 9. Fe-Ni-P phase diagrams edited from Romig and Goldstein (1980) at (a) 600°C, (b) 500°C, and (c) 400°C. The Löpönvaara meteorite is represented by the blue circle. At 600°C, Löpönvaara plots in the α + γ + Ph field; however, the meteorite is completely void of the γ phase. At lower temperatures, the meteorite plots in the α + Ph field. These phases are the two main constituents of the Löpönvaara meteorite.

the metal phase, leaving behind just α + Ph, as the meteorite does not contain taenite or rhabdites.

The textural features of Löpönvaara suggest that it likely crystallized relatively fast at low temperatures, below 600°C. Upon slow cooling (≪100°C Ma^{-1}), kamacite has time to grow large crystals with coarse hieroglyphic schreibersite. An example of meteorites that crystallized slowly from a P-rich, S-poor magma is the IIG irons: their slow crystallization resulted in the formation of very large homogeneous kamacite granules, with coarse-grained, hieroglyphic, and skeletal schreibersite inclusions (Wasson & Choe, 2009). However, upon fast solidification, the kamacite and schreibersite phases will retain an anhedral, fine-grained texture. Such fast cooling does not correlate with crystallization in a parent body with a mantled core, but rather in a large metallic body with scarcely any silicate insulation. This kind of crystallization environment may have formed e.g., as a result of grazing protoplanetary impact (e.g., Asphaug et al., 2006) and is supported by the fact that Löpönvaara does not contain any silicates. Furthermore, the brittle deformation of schreibersite and the substantial amounts of zoned troilite in the meteorite suggest that the meteorite's texture has a shock-induced origin. Pure troilite typically contains <1% elements other than FeS (Buchwald, 1975), but our results suggest that the troilite in Löpönvaara is very heterogeneous as it contains on average 11.1 wt% Ni and 0.6 wt% P in addition to 55.2 wt% Fe and 31.2 wt% S. When exposed to shock compression and associated with reheating, troilite melts easily at relatively low temperatures and can partially dissolve the encasing walls of schreibersite (Buchwald, 1975), which can result in compositionally heterogeneous troilite (Nichiporuk & Chodos, 1959).

Based on the data collected in this study, we suggest the following scenario based on the compositional and textural features of Löpönvaara: (1) possible occurrence of liquid immiscibility in the Löpönvaara parent body that is represented by the siderophile trace element depletion of Löpönvaara; (2) re-heating of the crystallized material possibly due to a shock event; (3) rapid crystallization that produced the unequilibrated texture and phases of the meteorite.

CONCLUSIONS

Our main conclusions are as follows:

1. The discovery of Löpönvaara increases the number of P-rich iron meteorites to eight and makes Löpönvaara the only P-rich iron with >3 wt% P.
2. Based on XRD and SEM–EDS data, Löpönvaara consists of two main meteoritic mineral phases: kamacite (α-(Fe, Ni)) and schreibersite ($(Fe,Ni)_3P$),

with minor amounts of troilite (FeS) and terrestrial oxidation products. Schreibersite occurs solely as matrix material. Kamacite occurs as rare large clasts, "mid-sized" ≤0.5 mm clasts, and exsolution blebs and globules in the matrix. Both schreibersite and the three types of kamacite are very homogeneous in composition, although the exsolved kamacite has a higher Fe:Ni ratio than the mid-sized clasts, and the rare large clasts contain significantly less P than the mid-sized clasts.

3. Liquid immiscibility possibly occurred in the Löpönvaara parent body, resulting in the extremely high concentration of P in Löpönvaara. The meteorite likely retained its original composition via late-stage fractional crystallization from the P-rich portion of immiscible magma.
4. The mineral assemblages and textural features suggest that Löpönvaara was re-heated, followed by rapid crystallization, likely due to a possible impact shock event on its parent body.

Acknowledgments—We thank Pekka Kokko, the discoverer of the Löpönvaara meteorite, for donating this unique find for research. Furthermore, the Materials Research Infrastructure (MARI) at the Department of Physics and Astronomy in the University of Turku is acknowledged for access to SEM–EDS and XRD instruments. Collaboration with the Finnish Geosciences Research Laboratory (SGL) regarding the LA-SC-ICPMS analyses is also acknowledged. We also thank Kevin Righter, Axel Wittmann, and an anonymous reviewer for their comments that helped us greatly improve the quality of this manuscript. Open access publishing facilitated by Abo Akademi, as part of the Wiley - FinELib agreement.

Data Availability Statement—Data that support the findings in this study is available in the Supporting Information.

Editorial Handling—Dr. Kevin Righter

REFERENCES

Asphaug, E., Agnor, C. B., and Williams, Q. 2006. Hit-and-Run Planetary Collisions. *Nature* 439: 155–160. https://doi.org/10.1038/nature04311.

Buchwald, V. F. 1975. *Handbook of Iron Meteorites*. Berkeley, CA: University of California Press. 1418.

Chiappe, E. M., Ash, R. D., Luttinen, A., Lukkari, S., Kuva, J., Hilton, C. D., and Walker, R. J. 2023. Chemical and Genetic Characterization of the Ungrouped Pallasite Lieksa. *Meteoritics & Planetary Science* 58: 1747–59. https://doi.org/10.1111/maps.14095.

Chiappe, E. M., Ash, R. D., and Walker, R. J. 2023. Age, Genetics, and Crystallization Sequence of the Group IIIE Iron Meteorites. *Geochimica et Cosmochimica Acta* 354: 51–61. https://doi.org/10.1016/j.gca.2023.06.009.

Doan, A. S., and Goldstein, J. I. 1969. The Formation of Phosphides in Iron Meteorites. In *Meteorite Research: Proceedings of a Symposium on Meteorite Research*, edited by P. M. Millman, 7–13. Vienna: Springer Netherlands. https://doi.org/10.1007/978-94-010-3411-1_62.

Doan, A. S., and Goldstein, J. I. 1970. The Ternary Phase Diagram, Fe-Ni-P. *Metallurgical Transactions* 1: 1759–67. https://doi.org/10.1007/BF02642026.

Esbensen, K. H., Buchwald, V. F., Malvin, D. J., and Wasson, J. T. 1982. Systematic Compositional Variations in the Cape York Iron Meteorite. *Geochimica et Cosmochimica Acta* 46: 1913–20. https://doi.org/10.1016/0016-7037(82)90129-6.

Garvie, L. A. 2012. The Meteoritical Bulletin, No. 99. *Meteoritics & Planetary Science* 47: 1887. https://doi.org/10.1111/maps.120572012.

Gattacceca, J., Bouvier, A., Grossman, J., Metzler, K., and Uehara, M. 2019. The Meteoritical Bulletin, No. 106. *Meteoritics & Planetary Science* 54: 469–471. https://doi.org/10.1111/maps.13215.

Gattacceca, J., McCubbin, F. M., Bouvier, A., and Grossman, J. N. 2020. The Meteoritical Bulletin, No. 108. *Meteoritics & Planetary Science* 55: 1146–50. https://doi.org/10.1111/maps.13493.

Gattacceca, J., McCubbin, F. M., Grossman, J. N., Schrader, D. L., Cartier, C., Consolmagno, G., Goodrich, C., et al. 2024. The Meteoritical Bulletin, No. 112. *Meteoritics & Planetary Science* 59: 1820–23. https://doi.org/10.1111/maps.14181.

Gattacceca, J., McCubbin, F. M., Grossman, J. N., Schrader, D. L., Cartier, C., Consolmagno, G., Goodrich, C., et al. 2025. The Meteoritical Bulletin, No. 113. *Meteoritics & Planetary Science* 60: 1587–91. https://doi.org/10.1111/maps.14374.

Goldstein, J. I., and Doan, A. S., Jr. 1972. The Effect of Phosphorus on the Formation of the Widmanstätten Pattern in Iron Meteorites. *Geochimica et Cosmochimica Acta* 36: 51–69. https://doi.org/10.1016/0016-7037(72)90120-2.

Groeneveld, D. 1959. A New Iron Meteorite from Bellsbank Barkly West District. *South African Journal of Geology* 62: 75–79.

Henderson, E. P., and Perry, S. H. 1948. Re-Examination of the Soper, Oklahoma Meteorite. *American Mineralogist: Journal of Earth and Planetary Materials* 33: 692–94.

Hilton, C. D., Ash, R. D., and Walker, R. J. 2020. Crystallization Histories of the Group IIF Iron Meteorites and Eagle Station Pallasites. *Meteoritics & Planetary Science* 55: 2570–86. https://doi.org/10.1111/maps.13602.

Hintenberger, H., Schultz, L., Wänke, H., and Weber, H. 1967. Helium- und Neonisotope in Eisenmeteoriten und der Tritiumverlust in Hexaedriten. *Zeitschrift Für Naturforschung. A, Astrophysik, Physik Und Physikalische Chemie* 22: 780–87. https://doi.org/10.1515/zna-1967-0527.

Hofmann, B. A., Lorenzetti, S., Eugster, O., Krähenbühl, U., Herzog, G., Serefiddin, F., Gnos, E., Eggimann, M., and Wasson, J. T. 2009. The Twannberg (Switzerland) IIG Iron Meteorites: Mineralogy, Chemistry, and CRE Ages. *Meteoritics & Planetary Science* 44: 187–199. https://doi.org/10.1111/j.1945-5100.2009.tb00727.x.

Jochum, K. P., Willbold, M., Raczek, I., Stoll, B., and Herwig, K. 2005. Chemical Characterisation of the USGS Reference Glasses GSA-1G, GSC-1G, GSD-1G, GSE-1G, BCR-2G, BHVO-2G and BIR-1G Using EPMA, ID-TIMS, ID-ICP-MS and LA-ICP-MS. *Geostandards and Geoanalytical Research* 29: 285–302.

Kotomaa, L. 2022. Classification of Iron Meteorites and Description of Mineralogy, Geochemistry, and Texture of the Lieksa-4 Meteorite. MSc thesis, University of Turku.

Kotomaa, L., Väisänen, M., O'Brien, H., Mäkilä, E., Peltola, A., and Kokko, P. 2023. Classification of the phosphorus-rich Lieksa 4 iron meteoriter. In *Abstracts of the 1st GeoDays*, edited by J. S. Heinonen, 86. Helsinki, Finland: Geological Society of Finland.

Kracher, A., Willis, J., and Wasson, J. T. 1980. Chemical Classification of Iron Meteorites—IX. A New Group (IIF), Revision of IAB and IIICD, and Data on 57 Additional Irons. *Geochimica et Cosmochimica Acta* 44: 773–787. https://doi.org/10.1016/0016-7037(80)90259-8.

Lodders, K., Bergemann, M., and Palme, H. 2025. Solar System Elemental Abundances from the Solar Photosphere and CI-Chondrites. *Space Science Reviews* 221: 23. https://doi.org/10.1007/s11214-025-01146-w.

Malvin, D. J., Wang, D., and Wasson, J. T. 1984. Chemical Classification of Iron Meteorites–X. Multielement Studies of 43 Irons, Resolution of Group IIIE from IIIAB, and Evaluation of Cu as a Taxonomic Parameter. *Geochimica et Cosmochimica Acta* 48: 785–804. https://doi.org/10.1016/0016-7037(84)90101-7.

Moutinho, A. L. R., Crosta, A. P., Navarro, M. S., Enzweiler, J., Silva, G. G., Scholz, R., Hill, P. J. A., et al. 2022. Three New Brazilian Iron Meteorites: Nova Olinda, Conceicao Do Tocantins and Augusto Pestana. *Meteoritics & Planetary Science* 57: 6477.

Nichiporuk, W., and Chodos, A. A. 1959. The Concentration of Vanadium, Chromium, Iron, Cobalt, Nickel, Copper, Zinc, and Arsenic in the Meteoritic Iron Sulfide Nodules. *Journal of Geophysical Research* 64: 2451–63. https://doi.org/10.1029/JZ064i012p02451.

Reed, S. J. B. 1965. Electron-Probe Microanalysis of Schreibersite and Rhabdite in Iron Meteorites. *Geochimica et Cosmochimica Acta* 29: 513–534. https://doi.org/10.1016/0016-7037(65)90044-X.

Romig, A. D., and Goldstein, J. I. 1980. Determination of the Fe-Ni and Fe-Ni-P Phase Diagrams at Low Temperatures (700 to 300 °C). *Metallurgical Transactions A* 11: 1151–59. https://doi.org/10.1007/BF02668139.

Romig, A. D., and Goldstein, J. I. 1981. The Diffusivity of Ni in fe-Ni and Fe-Ni-P Martensites. *Metallurgical Transactions A* 12: 243–251. https://doi.org/10.1007/BF02655197.

Ruzicka, A., Grossman, J., Bouvier, A., Herd, C. D., and Agee, C. B. 2015. The Meteoritical Bulletin, No. 101. *Meteoritics & Planetary Science* 50: 1661. https://doi.org/10.1111/maps.12490.

Scott, E. R., and Wasson, J. T. 1976. Chemical Classification of Iron Meteorites—VIII. Groups IC. IIE, IIIF and 97 Other Irons. *Geochimica et Cosmochimica Acta* 40: 103–115. https://doi.org/10.1016/0016-7037(76)90198-8.

Scott, E. R., Wasson, J. T., and Buchwald, V. F. 1973. The Chemical Classification of Iron Meteorites—VII. A Reinvestigation of Irons with Ge Concentrations between 25 and 80 ppm. *Geochimica et Cosmochimica Acta* 37: 1957–83. https://doi.org/10.1016/0016-7037(73)90151-8.

Tornabene, H. A., Ash, R. D., Walker, R. J., and Bermingham, K. R. 2023. Genetics, Age, and Crystallization History of Group IC Iron Meteorites. *Geochimica et Cosmochimica Acta* 340: 108–119. https://doi.org/10.1016/j.gca.2022.11.016.

Tornabene, H. A., Hilton, C. D., Bermingham, K. R., Ash, R. D., and Walker, R. J. 2020. Genetics, Age and Crystallization History of Group IIC Iron Meteorites. *Geochimica et Cosmochimica Acta* 288: 36–50. https://doi.org/10.1016/j.gca.2020.07.036.

Van Achterbergh, E., Ryan, C. G., Jackson, S. E., and Griffin, W. L. 2001. Data Reduction Software for LA-ICP-MS. In *Laser-Ablation-ICPMS in the Earth Sciences—Principles and Applications*, edited by P. J. Sylvester, 239–243. Canada: Mineralogical Association of Canada Short Course Series, St John, Newfoundland.

Walker, R. J., McDonough, W. F., Honesto, J., Chabot, N. L., McCoy, T. J., Ash, R. D., and Bellucci, J. J. 2008. Modeling Fractional Crystallization of Group IVB Iron Meteorites. *Geochimica et Cosmochimica Acta* 72: 2198–2216. https://doi.org/10.1016/j.gca.2008.01.021.

Wasson, J. T. 1990. Ungrouped Iron Meteorites in Antarctica: Origin of Anomalously High Abundance. *Science* 249: 900–902. https://doi.org/10.1126/science.249.4971.900.

Wasson, J. T. 1999. Trapped Melt in IIIAB Irons; Solid/Liquid Elemental Partitioning during the Fractionation of the IIIAB Magma. *Geochimica et Cosmochimica Acta* 63: 2875–89. https://doi.org/10.1016/S0016-7037(99)00283-5.

Wasson, J. T. 2011. Relationship Between Iron-Meteorite Composition and Size: Compositional Distribution of Irons from North Africa. *Geochimica et Cosmochimica Acta* 75: 1757–72. https://doi.org/10.1016/j.gca.2010.12.017.

Wasson, J. T. 2016. Formation of the Treysa Quintet and the Main-Group Pallasites by Impact-Generated Processes in the IIIAB Asteroid. *Meteoritics & Planetary Science* 51: 773–784. https://doi.org/10.1111/maps.12635.

Wasson, J. T. 2017. Formation of Non-magmatic Iron-Meteorite Group IIE. *Geochimica et Cosmochimica Acta* 197: 396–416. https://doi.org/10.1016/j.gca.2016.09.043.

Wasson, J. T., and Choe, W. H. 2009. The IIG Iron Meteorites: Probable Formation in the IIAB Core. *Geochimica et Cosmochimica Acta* 73: 4879–90. https://doi.org/10.1016/j.gca.2009.05.062.

Wasson, J. T., Choi, B. G., Jerde, E. A., and Ulff-Møller, F. 1998. Chemical Classification of Iron Meteorites: XII. New Members of the Magmatic Groups. *Geochimica et Cosmochimica Acta* 62: 715–724. https://doi.org/10.1016/S0016-7037(97)00379-7.

Wasson, J. T., and De Bon, C. C. 1998. New Chilean Iron Meteorites: Medium Octahedrites from Northern Chile Are Unique. *Meteoritics & Planetary Science* 33: 175–79. https://doi.org/10.1111/j.1945-5100.1998.tb01623.x.

Wasson, J. T., and Huber, H. 2006. Compositional Trends among IID Irons; Their Possible Formation from the P-Rich Lower Magma in a Two-Layer Core. *Geochimica et Cosmochimica Acta* 70: 6153–67. https://doi.org/10.1016/j.gca.2006.01.032.

Wasson, J. T., Huber, H., and Malvin, D. J. 2007. Formation of IIAB Iron Meteorites. *Geochimica et Cosmochimica Acta* 71: 760–781. https://doi.org/10.1016/j.gca.2006.09.032.

Wasson, J. T., and Kallemeyn, G. W. 2002. The IAB Iron-Meteorite Complex: A Group, Five Subgroups, Numerous Grouplets, Closely Related, Mainly Formed by Crystal Segregation in Rapidly Cooling Melts. *Geochimica et Cosmochimica Acta* 66: 2445–73. https://doi.org/10.1016/S0016-7037(02)00848-7.

Wasson, J. T., Ouyang, X., Wang, J., and Eric, J. 1989. Chemical Classification of Iron Meteorites: XI. Multi-Element Studies of 38 New Irons and the High Abundance of Ungrouped Irons from Antarctica. *Geochimica et Cosmochimica Acta* 53: 735–744. https://doi.org/10.1016/0016-7037(89)90016-1.

Wasson, J. T., and Richardson, J. W. 2001. Fractionation Trends among IVA Iron Meteorites: Contrasts with IIIAB Trends. *Geochimica et Cosmochimica Acta* 65: 951–970. https://doi.org/10.1016/S0016-7037(00)00597-4.

Wasson, J. T., and Schaudy, R. 1971. The Chemical Classification of Iron Meteorites—V Groups IIIC and IIID and Other Irons with Germanium Concentrations between 1 and 25 Ppm. *Icarus* 14: 59–70. https://doi.org/10.1016/0019-1035(71)90102-3.

Weisberg, M. K., Smith, C., Benedix, G., Herd, C. D. K., Righter, K., Haack, H., Yamaguchi, A., Aoudjehane, H. C., and Grossman, J. N. 2009. The Meteoritical Bulletin, No. 96. *Meteoritics & Planetary Science* 44: 1355–97. https://doi.org/10.1111/j.1945-5100.2009.tb01227.x.

Zhang, B., Chabot, N. L., Rubin, A. E., Humayun, M., Boesenberg, J. S., and van Niekerk, D. 2022. Chemical Study of Group IIIF Iron Meteorites and the Potentially Related Pallasites Zinder and Northwest Africa 1911. *Geochimica et Cosmochimica Acta* 323: 202–219. https://doi.org/10.1016/j.gca.2022.02.004.

SUPPORTING INFORMATION

Additional supporting information may be found in the online version of this article.

Figure S1. X-ray diffractograms of (a) round, metallic clasts, and (b) brittle matrix. The patterns correspond to kamacite (α-(Fe,Ni)) and schreibersite ($(Fe,Ni)_3P$). Typical peaks are labeled by the Miller indices calculated using Match! Software (Crystal Impact).

Table S1. Scanning electron microscope–energy dispersive spectroscopy (SEM–EDS) standardized spectral analysis results for mid-sized kamacite.

Table S2. Scanning electron microscope–energy dispersive spectroscopy (SEM–EDS) standardized spectral analysis results for exsolved kamacite.

Table S3. Scanning electron microscope–energy dispersive spectroscopy (SEM–EDS) standardized spectral analysis results for schreibersite.

Table S4. Scanning electron microscope–energy dispersive spectroscopy (SEM–EDS) standardized spectral analysis results for troilite.

Table S5. Laser ablation single collector inductively coupled plasma mass spectrometry (LA-SC-ICPMS) results for mid-sized kamacite, with Fe^{57} as internal standard.

Table S6. Laser ablation single collector inductively coupled plasma mass spectrometry (LA-SC-ICPMS) results for schreibersite, with Fe^{57} as internal standard.